10.1109/ULTSYM.2012.0058

Quantitative ultrasound techniques and improvements to diagnostic ultrasonic imaging

Michael L. Oelze, *Senior Member, IEEE*

Abstract— **Conventional ultrasound B-mode imaging is mainly qualitative in nature. While conventional imaging techniques, including ultrasound, may be sensitive to the detection of anomalous tissue features, the ability to classify these tissues often lacks specificity. As a result, a large number of biopsies of tissues with suspicious image findings are performed each year with a vast majority of these biopsies resulting in a negative finding. Quantitative ultrasound (QUS) imaging techniques can provide specific numbers related to tissue features that can increase the specificity of image findings leading to improvements in diagnostic ultrasound. QUS imaging techniques can encompass a wide variety of techniques including spectral-based parameterization, elastography, flow estimation and envelope statistics. Furthermore, a goal of QUS imaging techniques is to provide system- and operator-independent parameters related to tissue properties. Different applications of QUS imaging techniques in diagnostic ultrasound will be discussed in this paper. Specifically, spectral-based techniques and envelope statistics at clinical frequencies and at high ultrasonic frequencies (> 15 MHz) will be examined for their abilities to improve diagnostic ultrasound. Spectral-based techniques include the estimation of the backscatter coefficient, estimation of attenuation, and estimation of scatterer properties such as the correlation length associated with an effective scatterer size and the concentration of scatterers. Envelope statistics include the estimation of the number density of scatterers and quantification of coherent to incoherent signals produced from the tissue. Challenges related to the implementation of QUS imaging techniques and recent successes of QUS implementation for medical diagnostics will be discussed. Challenges for clinical application include correctly accounting for attenuation effects and implementation of QUS on clinical devices. Successful applications demonstrating the ability of QUS to improve medical diagnostics will include cancer detection and classification of solid tumors and lymph nodes, detection and quantification of fatty liver disease, and monitoring and assessment of thermal therapy on solid tumors.**

***Index Terms*—Backscatter coefficients, envelope statistics, quantitative ultrasound, tissue characterization.**

I. Introduction

Imaging has transformed the practice of medicine since the first X-rays were produced more than a 100 years ago [1]. Since that time medical imaging techniques have continued to evolve in their capabilities and have grown in their importance to medical practice. X-ray, X-ray CT, MRI, ultrasound, nuclear imaging, and optical imaging techniques have all been adapted for specific applications in medicine. Each of these imaging modalities has associated tradeoffs in terms of spatial resolution, frame rate, contrast, and imaging depth. New imaging techniques seek to improve one or more of these imaging features. The future of biomedical imaging lies in the continued improvement of imaging devices, developing multi-modality imaging techniques and developing quantitative imaging techniques.

The improvements in biomedical imaging have, for the most part, been beneficial to the practice of medicine. However, these advancements have not come without also producing new questions for the management of disease. In recent years, the high quality of imaging has resulted in high sensitivity to suspicious tissue features. Imaging technologies are very good at detecting small abnormalities. Unfortunately, these improvements in sensitivity have not always been paralleled by improvements in specificity. Modern biomedical imaging techniques are very good at identifying suspicious lesions or tissue structures but are not as good at specifying if an image finding is a result of a malignant or benign process. As a result, an "overdiagnosis" crisis has occurred [2, 3] in which many biopsies are being conducted because of suspicious image findings with the vast majority of these biopsies having negative findings [4]. Therefore, currently there is a need to improve medical imaging by improving the specificity of imaging techniques. Reducing the number of biopsies would reduce the cost of medical care, reduce the anxiety of and additional risks posed to patients undergoing these procedures, and reduce the time burden of physicians and pathologists.

In order to improve the specificity of biomedical imaging, quantitative imaging techniques have been developed. By providing specific numbers related to tissue structure or function in an imaging technique, the hope is that the additional information can produce higher specificity about the state of the tissue. In ultrasound, quantitative ultrasound (QUS) techniques include spectral-based parameterization of ultrasound signals, flow estimation through Doppler, tissue elastography techniques, shear wave imaging and envelope statistics. Some of these techniques have already been adopted on clinical devices while some of these techniques are still under development. In this paper, spectral-based

Manuscript received October 1, 2012. (This work was supported in part by grants from the National institutes of Health (NIH): R21CA139095, F32CA96419, R01CA111289, R21CA139095 and R01EB008992.

M. L. Oelze is with the Electrical and Computer Engineering Department, University of Illinois at Urbana-Champaign, Urbana, IL 61822, USA (e-mail: oelze@illinois.edu).

parameterization and envelope statistics will be explored for their ability to produce new sources of contrast and provide improved diagnostic potential for several disease states. These techniques are still under development and not available on current clinical ultrasound imaging systems, but have demonstrated success in specific applications. Successes of QUS in breast cancer detection, thyroid cancer diagnosis, diffuse liver disease quantification, detection of micrometastases in lymph nodes, and monitoring thermal therapies will be discussed in the paper along with current roadblocks to clinical translation of these technologies.

II. Theory

A. Spectral-Based Parameters

Spectral imaging techniques in ultrasound are based on obtaining a good representation of the power spectrum of the backscattered signal through the periodogram. The estimate of the power spectrum is normalized by taking into account the scattering volume and the characteristics of the transducer and excitation pulse. The backscatter coefficient (BSC) is related to the normalized power spectrum and is a fundamental property of the tissue medium. The BSC can be used as the basis for spectral-based QUS estimates and is given by [5],

$$\sigma_{bsc}(f) = \frac{R^2}{V}\frac{\langle I_{sc}(f)\rangle}{I_{inc}(f)} \propto W(f) \tag{1}$$

where R is the distance to the scattering volume of interest, V is the scattering volume defined by the beamwidth and range gate length, $I_{sc}(f)$ and $I_{inc}(f)$ are the scattered and incident fields, respectively, and $W(f)$ is the normalized power spectrum. Because the BSC is a fundamental property of the tissue, the BSC is both operator and system independent. In regions where the scattering is uniform, the BSC can be parameterized to yield estimates of the scatterer properties, which can then provide a geometrical interpretation of the underlying tissue microstructure.

To normalize the power spectra used in calculating the BSC, two different methods have been developed: 1) a planar reference method when using single-element transducers and 2) a reference phantom technique when using clinical array systems. In each method a region of interest (ROI) is defined to outline the tissue region to be analyzed and data blocks are defined corresponding to different spatial locations in the tissue ROI. The data blocks consist of windowed RF backscattered data. The sizes of the data blocks in the axial direction are normalized to the number of pulse lengths and in the lateral direction to the number of beamwidths. In our works we typically choose data blocks to be 10 pulse lengths by five beamwidths (50 resolution cells) [6].

In the planar reference technique, a smooth Plexiglas plate with known reflectivity was used to provide a reference signal from the surface. The normalized power spectrum is given by [7]

$$W(f) = \frac{1}{N}\frac{\Re^2}{4}A(f,L)\sum_{n=1}^{N}\frac{|S_n(f)|^2}{|S_{ref}(f)|^2} \tag{2}$$

where N represents the number of lateral scan lines used in the data block, $A(f,L)$ is an attenuation compensation function, $\Re$ is the reflection coefficient of the Plexiglas, and $S_n(\omega)$ and $S_{ref}(\omega)$ are the frequency domain signals from the sample for the nth scan line and the reference, respectively.

In the reference phantom technique, Yao et al. [8] derived the BSC from a sample by comparing the echo data acquired from the sample with the data from a well-characterized reference phantom whose BSCs and attenuation coefficients are known. The BSC using the reference phantom technique is given by

$$\sigma_b^s(\omega) = \sigma_b^{RPM}(\omega)e^{-4z[\alpha_{RPM}(\omega)-\alpha_s(\omega)]}\frac{|S_s(\omega)|^2}{|S_{RPM}(\omega)|^2} \tag{3}$$

where z is the depth, $\sigma_b^s(\omega)$ and $\alpha_s(\omega)$ are the backscatter and attenuation coefficients of the sample, respectively. Similarly, $\sigma_b^{RPM}(\omega)$ and $\alpha_{RPM}(\omega)$ are the backscatter and attenuation coefficients of the reference sample, respectively. The frequency domain signal from the sample and the reference sample are denoted by $S_s(\omega)$ and $S_{RPM}(\omega)$, respectively. This technique is applicable for any transducer geometry such as single-element focused/unfocused transducer and array systems.

Several studies have been conducted to demonstrate the ability to accurately estimate the BSC from tissue mimicking phantoms using multiple platforms [9-12]. These studies and studies in rat tumors demonstrated that the BSC can be accurately determined in a system-independent manner [10]. The accurate estimation of attenuation using multiple clinical machines, which is needed to compensate for frequency-dependent losses, was also demonstrated in one study [11]. Therefore, progress in QUS has demonstrated the ability of current clinically available ultrasound scanners to produce accurate and system-independent estimates of the BSC and attenuation.

Estimates of the scatterer properties (i.e., effective scatterer diameter (ESD) and effective acoustic concentration (EAC)) can be obtained by using an estimator that compares the BSC calculated from measurements to a theoretical BSC and minimizes some cost function versus trial values of ESD and EAC. In most instances, an estimator will provide a single value for the ESD. However, this value may represent a distribution of scatterer sizes and the width and shape of this scatterer size distribution will influence the final ESD estimate [13]. Different estimators can be used to reduce the effects of scatterer size distribution on the final ESD estimate [14]. The most common estimator in use for ESD and EAC calculation is the minimum average squared deviation (MASD) which

minimizes the average squared difference between the measured BSC and a theoretical BSC [5],

$$\text{ESD} = \min_{ESD}\left\{\frac{1}{M}\sum_{n=1}^{M}\left(X_n - \overline{X}\right)^2\right\} \quad (4)$$

where M is the number of data points in the analysis bandwidth, $X = 10\log_{10}\left[\hat{\sigma}_{bsc}/\sigma_{bsc}\right]$, where the '^' designates the estimated value and

$$\overline{X} = \frac{1}{M}\sum_{n=1}^{M} X_n \,. \quad (5)$$

Different trials values of the ESD are chosen over a range of values and the estimate is chosen that minimizes the error between the estimated BSC and the theoretical BSC. The $\overline{X}$ represents a gain factor between the estimated and theoretical BSC. Once the estimate of ESD is recovered, $\overline{X}$ can be used to calculate the estimate of the EAC.

B. Envelope Statistics

In the studies cited in this paper, envelope statistics were estimated from the homodyned K distribution,

$$p_A(A) = A\int_0^\infty xJ_0(sx)J_0(Ax)\left(1+\frac{x^2\sigma^2}{2\mu}\right)^{-\mu} dx \,. \quad (6)$$

To estimate the parameters of the homodyned K distribution, an algorithm was developed [15]. The algorithm made use of fractional order moments of the envelope SNR (R), skewness (S) and kurtosis (K) to provide estimates of the k (ratio of coherent to incoherent signal due to scattering) and μ (number of scatterers per unit resolution cell) parameters. The statistical parameter of the envelope are given by

$$R = \frac{E[A^\nu]}{\left(E[A^{2\nu}] - E^2[A^\nu]\right)^{1/2}} \quad (7)$$

$$S = \frac{E[A^{3\nu}] - 3E[A^\nu]E[A^{2\nu}] + 2E^3[A^\nu]}{\left(E[A^{2\nu}] - E^2[A^\nu]\right)^{3/2}} \quad (8)$$

$$K = \frac{E[A^{4\nu}] - 4E[A^\nu]E[A^{3\nu}] + 6E[A^{2\nu}]E^2[A^\nu] - 3E^4[A^\nu]}{\left(E[A^{2\nu}] - E^2[A^\nu]\right)^2} \quad (9)$$

where ν is an arbitrary moment order. A crucial observation is that if the amplitude is modeled according to the homodyned K distribution, then R, S, and K are functions of only k, μ, and ν. Thus, for a given value of ν, R, S, and K as defined in equations (7)-(9) do not depend on the specific values of s and σ, only on μ and the ratio $k = s/\sigma$.

By estimating R, S, and K for a given value of ν from ultrasonic echo data, it is possible to obtain estimates of k and μ. Rather than directly applying equations (7)-(9) to data to obtain these estimates, standard statistical techniques are used to obtain unbiased estimates. A single R, S, or K estimate will not uniquely identify the desired parameters k and μ because there are usually infinitely many points in (k,μ) space where the theoretical value equals the estimate. In fact, the locus of such points forms a curve in (k,μ) space which will be referred to as a level curve. However, curves derived from the R, S, and K estimates will usually come close to intersecting at a point. Furthermore, level curves derived from different moment orders provide additional curves. By finding the point in (k,μ) space that is in some sense closest to the level curves, an estimate is obtained [16].

During estimation, the R, S, and K are estimated for a data block. The estimated R, S, and K are used to generate level curves for two sets of fractional order moments for different values of k and μ. These curves are generated through comparison with a theoretical evaluation of R, S, and K. The location where the level curves intersect in the (k,μ) space provides the estimate of k and μ.

III. Experimental Procedures

A. Breast Cancer

Studies were conducted to determine if QUS could differentiate between benign tumors and malignant, and between different kinds of malignant tumors in rodent models of breast cancer [7, 17, 18]. QUS analysis was conducted over a broad ultrasonic frequency range of 5 to 25 MHz. The first tumors examined were spontaneous mammary fibroadenomas in rats [7]. The second kind of tumor examined was from a commercially available tumor cell line, the 4T1 MMT carcinoma for mice (ATCC, Manassas, VA) [17]. The carcinoma cells were cultured in medium and then injected subcutaneously into the fatpad of balb/c mice. Tumors were grown to a little over a centimeter in size and then examined using QUS techniques. The third kind of tumor examined was a mammary sarcoma (EHS sarcoma (ATCC, Manassas, VA) for mice) [18]. Sarcoma cells were injected into mice (C57BL/6) and tumors were allowed to grow to a little over a centimeter in size before scanning.

B. Thyroid Lesions

A high-frequency ultrasonic scanning system was used to scan thyroids extracted from mice that had spontaneously developed thyroid lesions (cancerous or benign). Three sets of mice were acquired having different predispositions to developing thyroid anomalies. A fourth set of mice had no predispositions for developing thyroid anomalies and were used as controls. The first set of were balb/c mice that were not expected to develop thyroid lesions and could be used as controls. The second set of mice were from the Rb 1+/- mouse strain and acquired from the mouse cancer model repository at the National Cancer Institute (courtesy of the Jacks Lab at the Koch Institute for Integrative Caner Research at MIT) [19]. Approximately 50% of these mice will develop C-cell

adenomas or C-cell hyperplasia in the thyroid. These growths would typically be benign in nature. The third set of mice was from the TG-BRAF mouse line and acquired from the Fagin lab (Sloan-Kettering Institute for Cancer Research) [20]. These mice would develop papillary thyroid carcinomas (PTCs), i.e., the most common type of thyroid cancer. The fourth set of mice were acquired from Dr. Cheng's lab (Center for Cancer Research, NIH) [21] and consisted of mutant mice that had introduced a dominant negative mutant thyroid nuclear receptor gene, TRβPV, into the TRβ gene locus. As a result of this mutation, as the $TR\beta^{PV/PV}$ mice aged they developed metastatic thyroid tumors consistent with follicular (variant) pattern papillary thyroid carcinomas.

When a mouse was selected for scanning, the mouse was euthanized and both thyroid lobes were extracted along with a portion of the trachea. The thyroid lobes were placed in a tank of degassed 0.9% saline maintained at 37 °C for ultrasonic scanning. The ultrasonic scanning system consisted of a 40-MHz weakly-focused (f/3) single-element transducer (NIH High-frequencyTransducer Resource Center, University of Southern California,Los Angeles, CA, USA). The active element had a diameter of 3 mm. The transducer was operated using a Panametrics 5900 pulser/receiver (Olympus NDT, Waltham, MA). Backscattered waveforms were acquired with a with a PC via a 14-bit A/D card with 250 MHz sampling and were saved to a computer for post-processing. For most thyroids, more than a dozen slices of the thyroids were acquired by translating the transducer using a micropositioning system (Daedal, Inc, Harrisburg, PA) controlled with custom LabView (National Instruments, Austin, TX) software. Slices were taken at 1 mm apart across the thyroid and perpendicular to the axial direction of the trachea. For each slice a number of scan lines were acquired depending on the size of the thyroid and each scan line was separated by one beamwidth.

From the scan lines, the envelope was detected and a B-mode image was constructed of the thyroid lobes. For processing, custom Matlab (MathWorks, Natick, MA) software was used to draw ROIs in each slice corresponding to the actual thyroid lobes. Within the ROIs, data blocks were automatically selected for QUS analysis. Each data block was 0.5 mm by 0.5 mm with a 75% overlap in the axial and lateral directions. From each data block the BSC versus frequency was estimated by the method of Chen et al [22]. To correct for attenuation, estimates from different thyroids were estimated using insertion loss techniques. The mean attenuation value from the estimates from all the thyroids was 1.19 ± 0.256 dB/MHz/cm and this value was used for attenuation compensation when calculating the BSC.

C. Diffuse Liver Disease

Fresh liver samples were extracted from male New Zealand white rabbits. The rabbits had been on a special fatty diet. The basal diet contained 10% fat, 1% cholesterol, 0:11% Mg, 14% protein and 54% carbohydrates. One group of five rabbits was on the fatty diet for three weeks and another group of five rabbits for six weeks. Another group consisting of four rabbits on standard chow diet was used as a control for the study.

The rabbits were euthanized and the livers were immediately extracted from the body, submersed in 0.9% degassed saline solution and scanned using an ultrasonic transducer (20 MHz) within an hour after extraction. Attenuation and sound speed were estimated by through transmission measurements. The BSC was calculated to obtain spectral estimates using an analysis bandwidth of 8 to 15 MHz (clinical ultrasound frequency ranges). The ESD and EAC were calculated from the BSC. The k and μ parameters were estimated from the envelope statistics of the backscattered ultrasound. To correlate the QUS parameters with the grade of fatty liver, QUS parameters were compared to the total liver lipids. The total liver lipids were estimated by following Folch method. Results of QUS parameters were then plotted versus the lipid content per gram of liver.

Steatosis grade 1 is defined for livers with greater than 5% total lipid content. In the present study, 1.5%, 5.6% and 13.9% total lipid content were observed in livers from animals on normal diet, 3-weeks of fatty diet and 6-weeks of fatty diet, respectively. Therefore, we characterized a fatty liver using QUS with grades of negligible steatosis, grade 1 steatosis, and grade 2 steatosis.

D. Detecting Micro-metastases in Lymph Nodes

High-frequency ultrasound (> 20 MHz) and QUS techniques have been used to detect and localize small metastatic foci in human lymph nodes [23]. The detection of micrometastases from histology is a significant medical problem because lymph nodes are typically cut into small slices of a millimeter or larger and examined. If the micrometastases are not within the slice region, they can be easily missed. Therefore, there is a sampling problem for pathologists to find these micrometastases.

To provide pathologists with improved sampling of the lymph nodes for the detection of micrometastases, freshly excised lymph nodes from cancer patients undergoing lymphadectomy were examined using QUS with both spectral-based parameters and envelope statistics parameters. Three-dimensional volumes were scanned with a transducer having a center frequency of 25.6 MHz. Following ultrasound scanning, each lymph node was inked to recover the orientation for later comparison to QUS images. The lymph nodes were then cut in half, embedded, fixed, sectioned in 65 μm intervals, stained with H&E, and imaged optically with a high quality slide scanner. Metastatic regions were highlighted in each region by a pathologist.

To obtain the QUS parameter estimates, data blocks were defined as cylindrical volumes and signals from the cylindrical volumes were gated and processed for QUS. The cylindrical volumes had a 1-mm diameter and a 1-mm length. Spectral-based parameters included the ESD, EAC, spectral slope (SS), spectral intercept (SI), and mid-band fit (MBF). From the envelope statistics, the k and μ parameters were estimated from the homodyned K distribution and the m and Ω parameters were estimated from the Nakagami distribution. QUS images were constructed from voxels corresponding to the cylindrical data blocks.

E. Thermal Therapy Monitoring

In vivo studies were conducted to monitor high-intensity focused ultrasound (HIFU) application using QUS techniques.

Mouse mammary adenocarcinoma (MAT) tumors were exposed to HIFU to create lesions. A 1-MHz (f/1.2) focused single-element transducer was used for HIFU exposures and a clinical array imaging system (UltrasonixRP, L 14-5/38) was used to record rf signals during the treatment. The BSC was estimated from the data corresponding to the treatment region and two parameters were estimated from the backscatter coefficient (ESD and EAC) and two parameters were estimated from the envelope statistics (k and μ) of the backscattered echoes.

The tumors were exposed to a spatial peak temporal average intensities (I_{SPTA}) of 335 W/cm^2 with 75% duty cycle, as measured in degassed water using a needle hydrophone (Precision Acoustics, Dorchester, UK). Data was collected using the clinical system during the exposure by synchronizing the capture of the rf data with periods between HIFU exposure tone-bursts. Exposure time of 60 sec was used in all the experiments.

B-mode images of the scanned areas were constructed. ROIs in the B-mode images and data blocks of size 10λ by 10λ (λ is the wavelength) were constructed with 80% overlap between adjacent data blocks both in the vertical and horizontal directions. Spectral-based parameters and envelope statistics were estimated for each data block for each frame acquired during the therapy. These parameters were then compared to temperature readings from a thermocouple placed behind the tumor. The placement of the thermocouple behind the tumor placed it outside of the HIFU beam focus and therefore represents a lower bound for the actual temperature in the treatment area.

IV. Results

A. Breast Cancer

The QUS parameters were used to distinguish and classify the three kinds of rodent models of mammary cancer. For the parameters, statistically significant differences were observed between the three kinds of tumors examined [24]. The parameters were related to underlying tissue structures by comparing to optical photomicrographs of the tumors. For example, the glandular acini in the fibroadenoma were identified as the dominant sources of scattering in the fibroadenomas [25] and cells were identified as prominent scatterers in the carcinomas and sarcomas. Figure 1 shows examples of QUS images of the tumors using the ESD parameter. The benign fibroadenoma provided a large contrast to the malignant tumors.

In addition, the use of a multiparameter set was observed to lead to improved classification of tumors as opposed to using one or two parameters. Figures 2a and 2b show feature analysis plots of QUS estimates for the carcinomas and sarcomas. When two parameters were used (Fig. 2a), statistically significant differences could be observed between all tumors and normal healthy tissues, however, overlap existed between the carcinomas and sarcomas. When three parameters were used (Fig. 2b), no overlap existed between the carcinomas and sarcomas allowing a clear distinction between the tumors based on the QUS parameters. As more parameters are added yielding a higher dimensional set, the ability to separate tissues can increase.

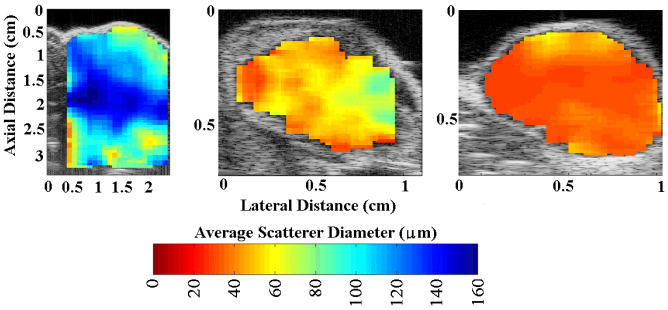

Fig. 1. Ultrasound grey-scale B-mode images superimposed with estimates of ESD for (left) rat fibroadenomas, (center) mouse carcinomas, and (right) mouse sarcomas.

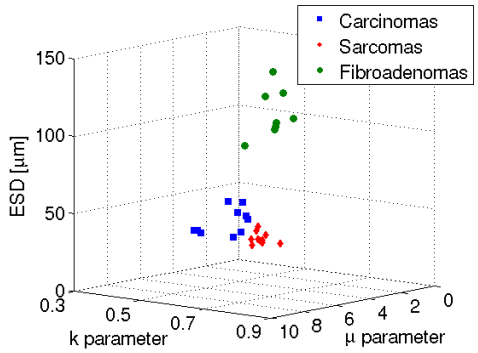

Fig. 2. Feature analysis plot of the ESD versus μ versus *k* parameter.

B. Thyroid Lesions

Figure 3 shows B-mode images of mice thyroids (normal and cancerous) along with QUS images enhanced by either the ESD or EAC. From B-mode images it would be difficult to differentiate between different thyroids based on their visible appearance. However, using the QUS images, differentiating between the malignant and cancerous cases is possible. However, the benign C-cell adenoma could not be differentiated from the normal thyroids based on the appearance of the QUS images.

Statistically significant differences were estimated using a one way analysis of the variance (ANOVA). Table I lists the p-values associated with the different sets of tumors and if statistically significant differences ($p < 0.05$) were observed between the different kinds of thyroids scanned. Statistically significant differences were observed between the cancerous thyroids (PTC and FTC) and the normal thyroids using the ESD, EAC, and μ parameters. The *k* parameter did not yield statistically significant differences between groups. No parameter was able to differentiate the C-cell adenomas from the normal thyroids. Only the ESD and EAC could differentiate the cancerous thyroids from the C-cell adenomas. Finally, the ESD and EAC provided the ability to distinguish the PTC from the FTC. The μ parameter did not provide statistically significant differences between the PTC and FTC thyroids.

TABLE I. TESTS OF STATISTICALLY SIGNIFICANT DIFFERENCES BETWEEN GROUPS FOR THE DIFFERENT PARAMETERS.

	Normal			C-Cell			PTC		
	ESD	EAC	μ	ESD	EAC	μ	ESD	EAC	μ
C-Cell	0.74	0.37	0.35						
PTC	< 0.05	< 0.05	< 0.05	< 0.05	< 0.05	0.94			
FTC	< 0.05	< 0.05	< 0.05	< 0.05	< 0.05	0.84	< 0.05	< 0.05	0.80

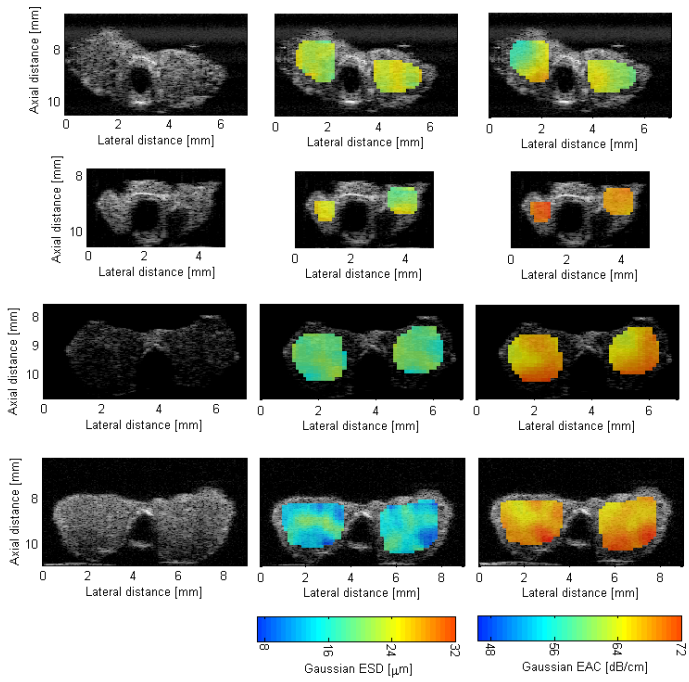

Fig. 3. B-mode (left column) and QUS images of thyroids enhanced by ESD (middle column) and EAC (right column). The top row is a normal thyroid (no tumor observed), the second row is a C-cell adenoma, the third row is PTC, and the last row is a FTC.

C. *Diffuse Liver Disease*

The BSCs were estimated from liver samples extracted from animals on normal diet, three weeks of fatty diet and six weeks of fatty diet as shown in Fig. 4. From BSCs additional parameters were estimated (ESD and EAC). The abilities of the QUS parameters to differentiate between degrees of fatty liver, as confirmed by lipid level content, were assessed through a one-way ANOVA. Statistically significant differences were quantified through a p-value < 0.5. The ESD decreased significantly and EAC increased with increasing lipid content, (the ESD is shown in Fig. 5 (a)). Specifically, the mean ESD was observed to be 30 μm, 25 μm and 19 μm in liver samples from animals on normal diet, three weeks of fatty diet and six weeks of fatty diet, respectively. The *k* parameter estimated from the liver samples of animals on normal diet and fatty diet did not provide statistically significant differences. However, the μ parameter, which is related to the density of scatterers per resolution cell, increased significantly with increasing lipid content, as shown in Fig. 5(b).

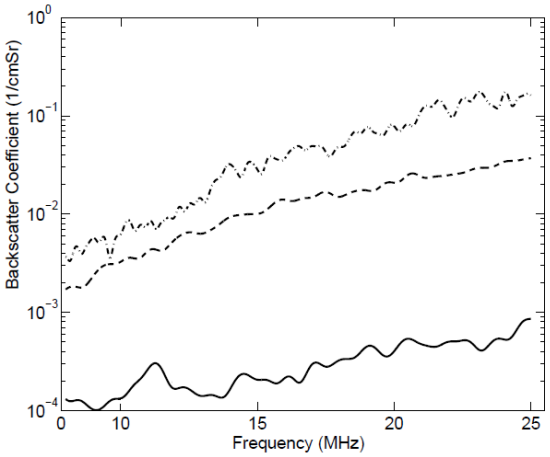

Fig. 4. Backscatter coefficients from liver samples extracted from animals on different diets with (solid line) zero days on fatty diet, (dashed line) three weeks on fatty diet, and (dot-dashed line) six weeks on fatty diet.

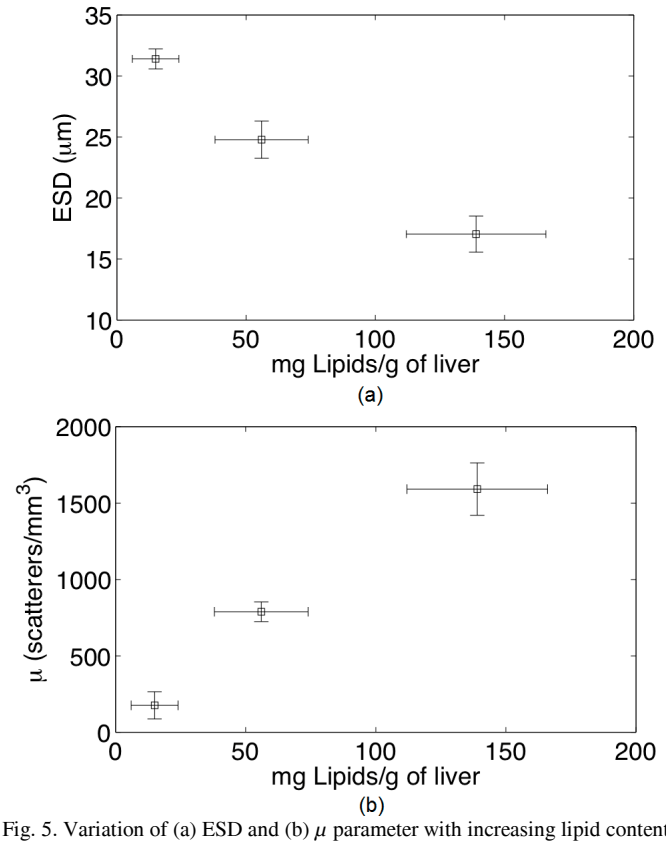

Fig. 5. Variation of (a) ESD and (b) μ parameter with increasing lipid content of the rabbit liver.

D. *Detecting Micro-metastases in Lymph Nodes*

In one study of 112 lymph nodes, a total of 13 combinations of the parameters were examined to build a classifier [23]. From this analysis it was observed that the ESD alone yielded a sensitivity and specificity of 95% and 91.3%, respectively. Receiver operator characteristic (ROC) curves were also generated and an area under the ROC curve (AUC) for the ESD parameter was found to be 0.986. The best classification was observed when combing the ESD with the *k* parameter with a 95%, 95.7%, and 0.996 sensitivity, specificity and

AUC, respectively. Therefore, QUS has demonstrated success at detecting micrometastases in human lymph nodes.

E. Thermal Therapy Monitoring

Two examples of the B-mode images of the tumors at different time points of HIFU application are shown in Figs. 6 and 7 (a), (d) and (g) and the corresponding parametric images enhanced by ΔEAC are shown in Figs. 6 and 7 (b), (e) and (h). The temperature profiles recorded by the thermocouple are shown as the blue curves in Figs. 6 and 7 (c), (f) and (i). The red circles indicate the time points corresponding to the displayed B-mode and parametric images. The three rows in the figure represent the results at three different time points of 0 sec, 60 sec and 80 sec, respectively during the treatment. The percentage changes in ΔEAC(%) are shown in Figs. 6 and 7 (c), (f) and (i) denoted in green color. The percentage changes in EAC versus time were estimated using

$$\Delta EAC(10\ \text{sec}) = \frac{EAC(10\ \text{sec}) - EAC(0\ \text{sec})}{EAC(\ \text{sec})}. \qquad (10)$$

An attenuation correction of 0.4 dB/cm/MHz was used to obtain the BSCs at different time points of HIFU application. It is expected that the lesion created by the HIFU application will have spatially varying attenuation, but the current results shown do not account for attenuation changes in the lesion.

The B-mode images in Fig. 6 do not show visible B-mode brightening as the HIFU therapy is applied while the B-mode image in Fig. 7does show B-mode brightening as therapy is applied which persists even after the HIFU is turned off. In both cases, the EAC was observed to increase with increasing temperature and then decrease with decreasing temperatuer when the HIFU was turned off. Therefore, these curves indicate that BSC based parameters can be correlated to temperature changes induced in tissues during thermal treatment.

V. Discussion

QUS techniques have successfully demonstrated new contrast for detecting and identifying disease for a variety of clinically relevant applications. In addition, QUS techniques can provide sensitive parameters to track the elevation of temperature in tissue due to HIFU therapy. These techniques are system and operator independent. The quantitative values provided by these new techniques can be used to uniquely identify disease state in many cases potentially leading to improvements in specificity.

QUS techniques over the frequency range of 5 to 25 MHz based on spectral features and envelope statistics were demonstrated to be capable of differentiating benign from malignant tumors in rodent models of breast cancer. High frequency QUS techniques (25 to 45 MHz) were capable of differentiating thyroid cancer from normal or benign thyroid conditions in mouse models of cancer. QUS techniques (8 to 15 MHz) could differentiate and grade degrees of fatty liver in rabbit models of diffuse liver disease. High-frequency QUS techniques (40 MHz) have been used successfully to detect micrometastases in lymph nodes of humans. Using a clinical ultrasound scanner, QUS techniques have been used to monitor the temperature induced by HIFU treatment.

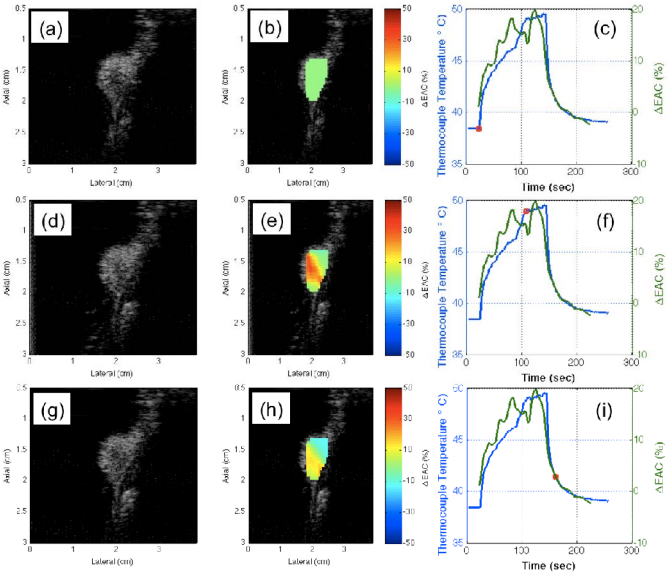

Fig. 6 B-mode and parametric images at different times during the HIFU treatment on rat R1.

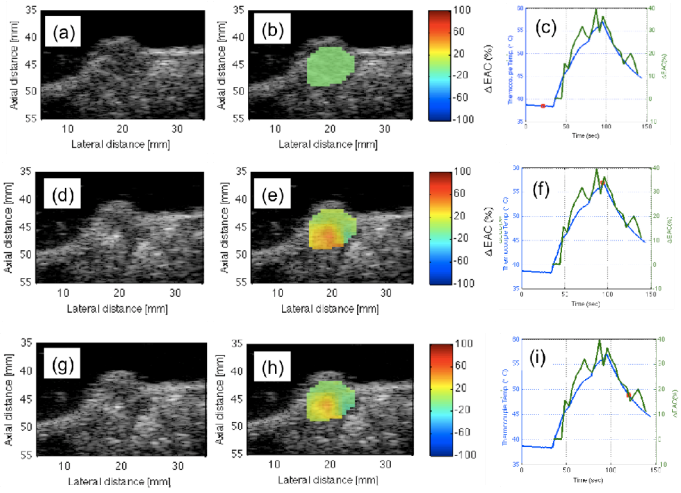

Fig. 7 B-mode and parametric images at different times during the HIFU treatment on rat R2.

While QUS techniques have demonstrated new contrast mechanisms for improving diagnostics for disease detection and classification, one significant roadblock has been identified for clinical implementation. That roadblock is the accurate compensation of frequency-dependent attenuation of the backscattered signals. Incorrectly accounting for attenuation effects will result in incorrect estimates of the BSC and incorrect estimates of the resolution cell size. Fortunately, a large amount of progress in estimation of attenuation from the backscatter has occurred over the last few years with several different algorithms being developed, tested and

validated [26-28]. These algorithms continue to evolve and studies have demonstrated the ability to estimate attenuation using multiple clinical scanners. Therefore, the main roadblock to clinical implementation of QUS techniques appears to be solved or close to being solved through the development of several new attenuation estimation algorithms. Furthermore, attenuation itself has high potential to provide an additional parameter with diagnostic value.

VI. Conclusion

QUS techniques have been developed that show high potential for improving diagnostic ultrasound for a number of different applications. The new sources of contrast and the ability to correlate specific quantitative values to tissue state will help improve medical diagnostics and improve specificity. Roadblocks to implementation on clinical devices have been largely overcome in recent years due to the work of several different groups. Therefore, QUS techniques are poised to significantly enhance biomedical ultrasonic imaging capabilities.

Acknowledgment

The author wishes to acknowledge the technical, scientific and professional assistance of William D. O'Brien Jr., Rita Miller, Sandhya Sarwate, Roberto Lavarello, Jonathan Mamou, Goutam Ghoshal. Jeremy Kemmerer, David Hruska, and Adam Luchies.

References

[1] Spiegel PK, The first clinical X-ray made in America – 100 years. *Amer J Roentgen*, 164, 241-243, 1995.

[2] Welch HG and CB William, Overdiagnosis in cancer. *J Natl Cancer Inst*, 102, 1-9, 2010.

[3] Esserman L and I Thompson, Solving the overdiagnosis dilemma. *J Natl Cancer Inst*, 102, 582-583, 2010.

[4] Silverstein M, Recht A, Lagois M, et al. Image-Detected Breast Cancer: State-of-the-Art Diagnosis and Treatment. *J Am Coll Surg*, 209:504-520, 2009.

[5] Insana MF, Wagner RF, Brown, DG, et al. Describing small-scale structure in random media using pulse-echo ultrasound. *J Acoust Soc Amer*, 87: 179-192, 1990.

[6] Oelze ML and O'Brien, Jr. WD. Defining optimal axial and lateral resolution for estimating scatterer properties from volumes using ultrasound backscatter. *J Acoust Soc Amer*, 115: 3226-3234, 2004.

[7] Oelze ML, Zachary JF, and O'Brien Jr. WD. Characterization of tissue microstructure using ultrasonic backscatter: Theory and technique for optimization using a Gaussian form factor. *J Acoust Soc Amer*, 112: 1202-1211, 2002.

[8] Yao LX, Zagzebski JA, and Madsen EL. Backscatter coefficient measurements using a reference phantom to extract depth-dependent instrumentation factors. *Ultrason Imaging*, 12: 58-70, 1990.

[9] Anderson JJ, Herd MT, King MR, et al. Interlaboratory comparison of backscatter coefficient estimates for tissue-mimicking phantoms. *Ultrason Imaging*, 32: 48-64, 2010.

[10] Wirtzfeld LA, Ghoshal G, Hafez ZT, et al. Cross-imaging platform comparison of ultrasonic backscatter coefficient measurements of live rat tumors. *J Ultrasound Med*, 29: 1117-1123, 2010.

[11] Nam K, Rosado-Mendez IM, Wirtzfeld LA, et al. Ultrasonic attenuation and backscatter coefficient estimates of rodent-tumor mimicking structures: Comparison of results among clinical scanners. *Ultrason Imaging*, 33: 233-250, 2011.

[12] Nam K, Rosado-Mendez IM, Wirtzfeld LA, et al. Cross-imaging system comparison of backscatter coefficient estimates from tissue-mimicking sample. *J Acoust Soc Amer*, 132: 1319-1324, 2012.

[13] Lavarello R and Oelze ML. Quantitative ultrasound estimates from populations of scatterer with continuous size distributions. *IEEE Trans Ultrason, Ferroelectr, Freq Contr*, 58: 744-753, 2011.

[14] Lavarello R and Oelze ML. Quantitative ultrasound estimates from populations of scatterers with continuous size distributions – Effects of size estimator algorithm. *IEEE Trans Ultrason, Ferroelectr, Freq Contr*, 59: 2066-2076, 2012.

[15] Hruska DP and Oelze ML. Improved parameter estimates based on the homodyned K distribution. *IEEE Trans Ultrason, Ferroelect, Freq Contr*, 56: 2471-2481, 2009.

[16] Hruska DP. Improved techniques for statistical analysis of the envelope of backscattered ultrasound using the homodyned K distribution. *M.S. Thesis, University of Illinois at Urbana-Champaign,* 2009.

[17] Oelze ML, Zachary JF, and O'Brien, Jr. WD. Differentiation and characterization of mammary fibroadenomas and 4T1 Carcinomas using ultrasound parametric imaging. *IEEE Trans Med Imag*, 23: 764-771, 2004.

[18] Oelze ML and Zachary JF. Examination of cancer in mouse models using quantitative ultrasound. *Ultrasound Med Biol*, 11: 1639-1648, 2006.

[19] Jacks T, A Fazeli, EM Schmitt, et al. Effects of an Rb mutation in the mouse. *Nature*, 359: 295-300, 1992.

[20] Knauf JA, X Ma, EP Smith, et al. Targeted expression of $BRAF^{V600E}$ in thyroid cells of transgenic mice results in papillary thyroid cancers that undergo dedifferentiation. *Cancer Res*, 65: 4238-4245, 2005.

[21] Suzuki H, MC Willingham, and S Cheng. Mice with a mutation in thyroid hormone receptor β gene spontaneously develop thyroid carcinoma: a mouse model of thyroid carcinogenesis. *Thyroid*, 12: 963-969, 2002.

[22] Chen X, D Phillips, KQ Schwarz, et al. The measurement of backscatter coefficient from a broadband pulse-echo system: a new formulation. *IEEE Trans Ultrason Ferroelectr Freq Contr*, 44: 515–525, 1997.

[23] Mamou J, A Coron, ML Oelze, et al. Three-Dimensional High-Frequency Backscatter and Envelope Quantification of Cancerous Human Lymph Nodes. *Ultrasound Med Biol*: 37, 345-357, 2011.

[24] Oelze ML, WD O'Brien, Jr., and JF Zachary. Quantitative ultrasound assessment of breast cancer using a multiparameter approach. *Proc IEEE Ultrasonics Symp*, New York, New York, 981-984, 2007.

[25] Oelze ML, JF Zachary, and WD O'Brien Jr. Parametric imaging of rat mammary tumors in vivo for the purposes of tissue characterization, *J Ultrasound Med*, 21: 1201-1210, 2002.

[26] Ghoshal G and Oelze ML. Attenuation estimation from time domain ultrasonic backscattered signals. *J Acoust Soc Amer*, 132: 533-543, 2012.

[27] Nam K, Zagzebski JA, Hall TJ. Simultaneous backscatter and attenuation estimation suing a least squares method with constraints. *Ultrasound Med Biol*, 37: 2096-2104, 2011.

[28] Labyed Y and Bigelow TA. A theoretical comparison of attenuation measurement techniques from backscattered ultrasound echoes. J Acoust Soc Amer, 129: 2316-2324, 2011.